Catalysis Surveys from Asia (2020) 24:134–142
https://doi.org/10.1007/s10563-020-09294-5

Effect of Ce Doping on Hydrothermal Stability of Cu-SAPO-18 in the Selective Catalytic Reduction of NO with NH_3

Qi Gao[1] · Qing Ye[1] · Shuai Han[1] · Shuiyuan Cheng[1] · Tianfang Kang[1] · Hongxing Dai[2]

Published online: 27 February 2020

Abstract
The Ce-Cu-SAPO-18 samples were prepared by the ion exchange method. Physicochemical properties of the samples were systematically characterized by a number of analytical techniques, and Ce doping and hydrothermal temperature effects on NH_3-SCR activity of Cu-SAPO-18 were also investigated. The results show that doping of Ce increased NH_3-SCR activity and hydrothermal stability of the Cu-SAPO-18 sample. After Ce doping, a more amount of the isolated Cu^{2+} ions entered the D6R and the catalyst structure was more stable. The structure and catalytic activity of Ce-Cu-SAPO-18 remained almost intact after hydrothermal aging at 650 °C. After hydrothermal aging at 850 °C, however, the structure of Ce-Cu-SAPO-18 was greatly destroyed, and its catalytic activity declined remarkably. The high-temperature hydrothermal aging treatment led to decreases in amount of the isolated Cu^{2+} ions and acidic sites, destroying in the zeolitic structure, and drop in NH_3-SCR activity.

Keywords Cu-SAPO-18 · Ce-Cu-SAPO-18 · Selective catalytic reduction · NH_3-SCR · Hydrothermal aging treatment

1 Introduction

Nitrogen oxides (NO_x) emitted from diesel exhaust are the main atmosphere pollutants [1]. NO_x mainly refers to NO and NO_2, which are harmful to human health, especially to the respiratory system [1]. Selective catalytic reduction of NO with ammonia (NH_3-SCR) has been widely used as one of the most effective technologies for the removal of NO_x from diesel engines [2–4], in which the core issue is the availability of high-performance catalysts. The commercial V_2O_5/WO_3-TiO_2 catalyst [5] has still many disadvantages, such as vanadium toxicity, narrow temperature window, and low hydrothermal stability [5], over which NH_3 can be oxidized at high temperatures to produce NO_x [6]. Therefore, there is an urgent need to develop efficient catalysts for NO_x removal that show excellent NH_3-SCR performance, wide temperature windows, and good hydrothermal stability, and high N_2 selectivity.

In recent decades, zeolites (e.g., SSZ-13 and SAPO-34) have received extensive attention because of their porous channel structures and high surface areas [7–10]. Cu-based zeolites with a CHA structure, such as Cu-SSZ-13 and Cu-SAPO-34, possess unique physicochemical properties. Among these porous materials, Cu-SSZ-13 has been commercially to apply for the NH_3-SCR of NO_x emitted from diesel exhaust [10–12]. The AEI structure is similar to the CHA structure [13]. According to a report [14], Cu-SAPO-18 with an AEI structure showed a high catalytic activity for NH_3-SCR. However, the overall activity of Cu-SAPO-18 needs to be further improved. Lanthanide-doped catalysts exhibit good oxygen storage ability and strong

Electronic supplementary material The online version of this article (https://doi.org/10.1007/s10563-020-09294-5) contains supplementary material, which is available to authorized users.

✉ Qing Ye
yeqing@bjut.edu.cn

✉ Hongxing Dai
hxdai@bjut.edu.cn

[1] Key Laboratory of Beijing on Regional Air Pollution Control, Department of Environmental Science, College of Environmental and Energy Engineering, Beijing University of Technology, Beijing 100124, China

[2] Beijing Key Laboratory for Green Catalysis and Separation, Key Laboratory of Beijing on Regional Air Pollution Control, Key Laboratory of Advanced Functional Materials, Education Ministry of China, and Laboratory of Catalysis Chemistry and Nanoscience, Department of Chemistry and Chemical Engineering, College of Environmental and Energy Engineering, Beijing University of Technology, Beijing 100124, China

redox properties [15]. It has been found that the doping of Ce to Cu-ZSM-5, Cu-SAPO-34 or Cu-SSZ-13 could improve the high-temperature hydrothermal stability and further broaden the operation temperature window [7, 16, 17]. In this work, we explore the effect of Ce doping on the NH_3-SCR performance and hydrothermal stability of Cu-SAPO-18.

2 Experimental

2.1 Catalyst Synthesis

According to the literature [18], we use *N*,*N*-diisopropylethylamine as a template agent to synthesize SAPO-18. Details of the preparation of SAPO-18 and NH_4-SAPO-18 were described in the Supplementary material.

Afterwards, an ion exchange method was employed to prepare the Ce-Cu-SAPO-18 samples, in which 1.0 g of NH_4-SAPO-18 was dispersed in 29 mL of $Cu(NO_3)_2$ aqueous solution and 29 mL of $Ce(NO_3)_3$ aqueous solution [19, 20]. In order to obtain the samples after the hydrothermal aging treatment, the samples were first treated in a 10 vol% H_2O-containing air flow (300 mL/min) at a ramp of 10 °C/min from 30 to 650, 750 or 850 °C, and then maintained at this temperature for 12 h.

Crystal structures of the samples were determined on an X-ray diffractometer (XRD) using Cu Kα radiation. The Cu and Ce contents in the samples were analyzed using an X-ray fluorescence spectrometer (XRF). X-ray photoelectron spectroscopy (XPS) was used to determine the binding energies of Cu 2p and Ce 2p as well as Cu and Ce concentrations on the surface of the samples. H_2 temperature-programmed reduction (H_2-TPR) and ammonia temperature-programmed desorption (NH_3-TPD) of the samples were carried out on the Builder PCA-1200 analyser. The in situ DRIFTS experiment was carried out on a Bruker TENSOR II spectrometer equipped with a smart collector and an MCT detector. For the NH_3 or NO adsorption experiments, the sample was exposed to a 500 ppm NO/N_2 flow or to a 500 ppm NH_3/N_2 flow. The NH_3 or NO adsorption spectrum of each sample was obtained by subtracting the background spectrum that was recorded by exposing the sample to a pure N_2 flow. The detailed characterization procedures can be seen from the Supplementary material.

2.2 Catalytic Activity Measurement

Catalytic activity evaluation of the samples was carried out in a microreactor. 150 mg of sample and 150 mg of quartz sand were mixed and put into the microreactor. NO concentrations at the inlet and outlet of the reactor were measured by a Thermo Model 42i-HL analyzer. The simulated exhaust gas was composed of 500 ppm NO, 500 ppm NH_3, 14 vol% O_2, 5 vol% H_2O, and N_2 (balance), and the total flow rate was 300 mL/min. The gas hourly space velocity (GHSV) was estimated to be 130,000 h^{-1}.

3 Results

3.1 NH_3-SCR Performance

NO conversions over the Ce-Cu-SAPO-18 samples with different Ce contents are shown in Fig. S1. The Cu-SAPO-18, Ce-Cu-SAPO-18 and Ce-SAPO-18 catalyst activity and partial characterization data in this article are quoted from our previous research [18]. The doping of Ce obviously enhanced catalytic activity of Cu-SAPO-18. Among the Ce-Cu-SAPO-18 samples with different Ce contents, the one containing 1.24 wt% Ce exhibited the widest reaction window and the best catalytic activity (NO conversions exceeded 90% at 200–550 °C). Therefore, the Ce-Cu-SAPO-18 sample with a Ce doping of 1.24 wt% was selected to investigate the hydrothermal stability. Figure 1 shows the NH_3-SCR performance of the fresh and 850 °C-aged Cu-SAPO-18 (denoted as Cu-SAPO-18–850) and the Ce-Cu-SAPO-18 samples with a Ce doping of 1.24 wt% at hydrothermal aging treatment (HAT) temperatures of 650, 750, and 850 °C (denoted as Ce-Cu-SAPO-18-650, Ce-Cu-SAPO-18-750, and Ce-Cu-SAPO-18-650, respectively). Obviously, compared with Cu-SAPO-18, catalytic activity of the Ce-Cu-SAPO-18

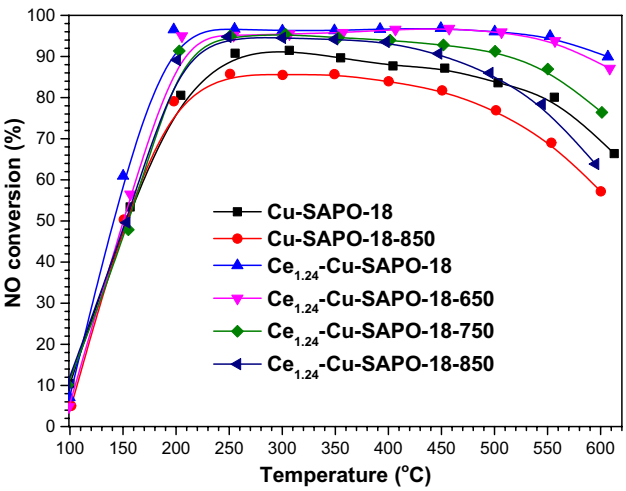

Fig. 1 NO conversion as a function of temperature for the NH_3–SCR reaction over the Cu-SAPO-18 and Ce-Cu-SAPO-18 samples before and after hydrothermal treatment at different temperatures. The reactant feed composition: 500 ppm NO, 500 ppm NH_3, 14% O_2, 5% H_2O, and N_2 (balanced); GHSV: 130,000 h^{-1}. Cu-SAPO-18, Ce-Cu-SAPO-18 catalyst activity data were obtained by our previous research ref. [18]

sample was better in the entire temperature range. Deactivation of the Ce-Cu-SAPO-18 was not observed after the hydrothermal aging treatment at 650 °C, wherein a NO conversion of more than 90% was maintained in the range of 250–500 °C. However, the activity at temperatures higher than 400 °C declined after hydrothermal aging at 750 °C. A further rise in hydrothermal aging temperature to 850 °C resulted in a significant decrease in NO conversion at high temperatures, possibly due to sintering of the active phase.

To further explore the role of Ce, hydrothermal stability of the Cu-SAPO-18 and Ce-Cu-SAPO-18 samples after the HAT at 850 °C were compared. As showed in Fig. 1, the fresh Cu-SAPO-18 sample exhibited high catalytic activity (NO conversion exceeded 90% at a temperature range of 250–450 °C). After the HAT at 850 °C, NO conversion decreased to less than 85% in the whole temperature range. Obviously, catalytic activity of the Ce-Cu-SAPO-18 sample was higher than that of the Cu-SAPO-18 sample after the HAT at 850 °C, indicating that doping of Ce to Cu-SAPO-18 considerably improved the hydrothermal stability. To better understand the role of Ce, the NH_3-SCR activities of SAPO-18, Ce-SAPO-18 and Ce-SAPO-18-850 samples are shown in Fig. S2. Compared with the SAPO-18 sample, catalytic activity of the Ce-SAPO-18 sample did not change significantly, indicating that when 1.24 wt% Ce was added, there were no more active sites added to the sample, but the interaction of Ce and Cu enhanced the NH_3-SCR performance of Ce-Cu-SAPO-18. The reasons for high hydrothermal stability of Ce-Cu-SAPO-18 were explained below.

3.2 XRD and BET Results

In order to explore effect of the HAT on the sample structure, XRD patterns of the Cu-SAPO-18 and Ce-Cu-SAPO-18 samples before and after the HAT were recorded, as shown in Fig. 2. Table 1 shows the BET surface area of each sample. Upon hydrothermal aging at 650 °C, the crystal structure and BET surface area of Ce-Cu-SAPO-18 were hardly changed. After hydrothermal aging at 750 °C, crystal structure was partially destroyed and BET surface area of the Ce-Cu-SAPO-18-750 sample decreased. However, crystal structure damage was serious when the HAT temperature rose to 850 °C, resulting in a sharp drop in surface area (e.g., from 597 m^2/g for fresh Cu-SAPO-18 to 304 m^2/g for Cu-SAPO-18-850 and 420 m^2/g for Ce-Cu-SAPO-18-850). Compared with the XRD and BET results of Ce-Cu-SAPO-18 after the HAT at 850 °C, the Cu-SAPO-18 sample was destroyed more seriously, indicating that introduction of Ce weakened damage of the sample structure induced after the high-temperature HAT process. That is to say, Ce doping was beneficial for maintaining the zeolitic structure of the sample after the HAT at high temperatures.

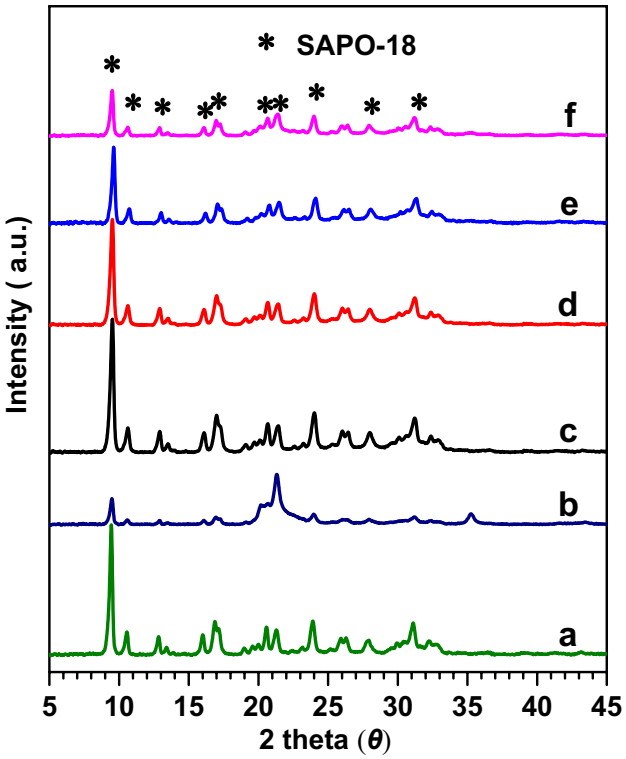

Fig. 2 Powdered XRD patterns of (a) Cu-SAPO-18, (b) Cu-SAPO-18-850, (c) Ce-Cu-SAPO-18, (d) Ce-Cu-SAPO-18-650, (e) Ce-Cu-SAPO-18-750, and (f) Ce-Cu-SAPO-18-850

3.3 NMR Results

In order to clarify the state of Al in the structure of the samples before and after the HAT, the ^{27}Al solid state NMR experiments were carried out. ^{27}Al MAS NMR spectra of the Ce-Cu-SAPO-18 samples before and after the HAT at different temperatures are shown in Fig. 3. Feature peaks at 38 ppm and −7 ppm were observed in these samples, which belonged to the framework tetrahedral Al and the extra-framework octahedral Al [8, 21], respectively. Upon hydrothermal aging at 650 °C, intensity of the tetrahedral Al signals in Ce-Cu-SAPO-18 did not change significantly. When the hydrothermal aging temperature increased to 750 °C, intensity of the tetrahedral Al signals in Ce-Cu-SAPO-18 decreased, especially that of the peak at 38 ppm dropped by ca. 13%. With a rise in hydrothermal aging temperature to 850 °C, peak intensity of the Ce-Cu-SAPO-18 samples decreased more significantly (e.g., the peak at 38 ppm decreased by ca. 23%).

To explore the effect of Ce doping on hydrothermal stability of Cu-SAPO-18, ^{27}Al MAS NMR spectra of the Cu-SAPO-18 and Ce-Cu-SAPO-18 samples before and after the

Table 1 Chemical compositions and BET surface areas of the fresh and hydrothermally aged Cu-SAPO-18 and Ce-Cu-SAPO-18 samples

Sample	Cu (wt%)	Ce (wt%)	Al (wt%)	P (wt%)	Si (wt%)	BET surface area (m^2/g)
Cu-SAPO-18	1.76	–	31.57	53.19	10.63	597
Cu-SAPO-18-850	–	–	–	–	–	304
Ce-Cu-SAPO-18	1.71	1.24	29.62	53.94	10.56	579
Ce-Cu-SAPO-18-650	–	–	–	–	–	510
Ce-Cu-SAPO-18-750	–	–	–	–	–	460
Ce-Cu-SAPO-18-850	–	–	–	–	–	420

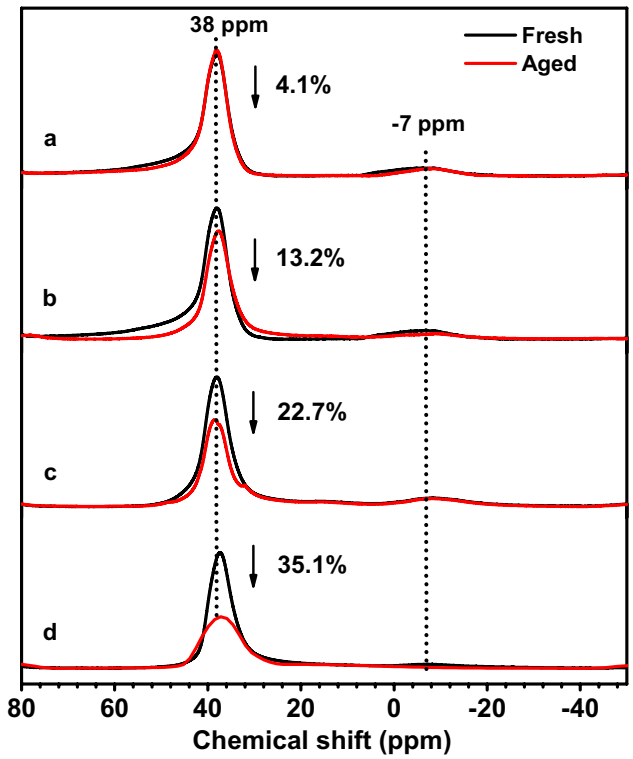

Fig. 3 Solid state ^{27}Al NMR spectra of (a) Ce-Cu-SAPO-18 and Ce-Cu-SAPO-18-650, (b) Ce-Cu-SAPO-18 and Ce-Cu-SAPO-18-750; (c) Ce-Cu-SAPO-18 and Ce-Cu-SAPO-18-850; (d) Cu-SAPO-18 and Cu-SAPO-18-850

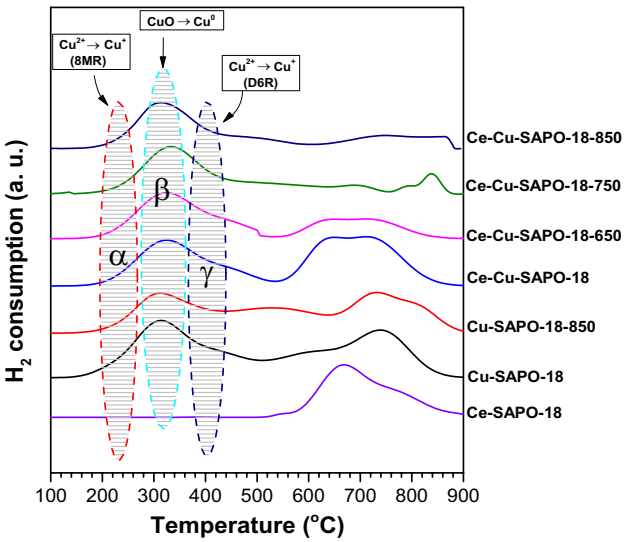

Fig. 4 H_2-TPR profiles of the Cu-SAPO-18 and Ce-Cu-SAPO-18 samples before and after the hydrothermal aging treatment

HAT at 850 °C are shown in Fig. 3. Intensity of the peak at 38 ppm of Cu-SAPO-18 decreased by 35.2% after the HAT at 850 °C, while the Ce-Cu-SAPO-18 sample only dropped by 22.7%. Apparently, dealumination of Cu-SAPO-18 was more serious after the HAT at 850 °C. Therefore, it is clear that the Ce addition can effectively reduce the dealumination in the hydrothermal aging process and promote the hydrothermal stability of the Cu-SAPO-18 sample, resulting in excellent SCR activity. Fan et al. [20] also reported that the introduction of a small amount of Ce or La into Cu-SAPO-34 during the hydrothermal aging process could effectively reduce the aggregation of copper and mitigate the dealumination progress of zeolite framework during the HAT process, hence maintaining the relatively high surface area and a uniform pore-size distribution of Cu-SAPO-34 sample. Based on the results of ^{27}Al solid state NMR, XRD, and BET characterization, compared with those in the Ce-Cu-SAPO-18-850 sample, dealumination and collapsing of the zeolitic structure were more serious in the Cu-SAPO-18 sample after the hydrothermal aging at 850 °C, which confirms that Ce doping could stabilize the framework Al in the sample.

3.4 Evolution of Cu Species

H_2-TPR technique was used to investigate the changes of reductive species in the samples before and after the HAT, and their profiles are shown in Fig. 4. There were three reduction peaks below 500 °C, which could be assigned to reduction of the Cu species [10, 22]. The peak (peak α) at ca. 220 °C belonged to reduction of the isolated Cu^{2+} ions near to the 8MRs cage [10], which was related to catalytic

activity of the sample in the SCR reaction at low temperatures. The peak (peak β) at 310 °C was attributed to reduction of the CuO to Cu^0 [22]. Another peak (peak γ) at 400 °C was considered to reduction of the Cu^{2+} ions in the D6R cage [10], which was closely associated with catalytic activity of the sample in the medium- and high-temperature range. In order to identify the reduction peak of Ce species in the sample, Cu-free Ce-SAPO-18 was also prepared and characterized by the H_2-TPR technique (Fig. 4). It can be seen that the reduction peak temperature of this sample exceeded 600 °C, which was attributed to reduction of the Ce species. Therefore, it can be inferred that the peak above 500 °C of Ce-Cu-SAPO-18 was partly due to reduction of the Ce species.

To further investigate the effect of the HAT on amount of the Cu species, the H_2-TPR peaks of the samples before and after the HAT were quantified via peak deconvolution, and their results are summarized in Table 2. After the HAT at 650 °C, amount of the total isolated Cu^{2+} species slightly decreased from 0.109 mmol/g for the fresh Ce-Cu-SAPO-18 sample to 0.103 mmol/g for the Ce-Cu-SAPO-18-650 sample. After the HAT at 750 °C, amount of the total isolated Cu^{2+} species in Ce-Cu-SAPO-18-750 decreased 0.082 mmol/g. When the HAT temperature increased to 850 °C, amount of the total isolated Cu^{2+} species significantly dropped to 0.073 mmol/g.

By Comparing amount of the total isolated Cu^{2+} ions in Ce-Cu-SAPO-18-850 (Fig. 4 and Table 2), that in Cu-SAPO-18 obviously decreased by 0.053 mmol/g (from 0.097 mmol/g in the fresh Cu-SAPO-18 sample to 0.044 mmol/g in the Cu-SAPO-18-850 sample), whereas there was a decrease of 0.036 mmol/g in the Ce-Cu-SAPO-18-850 sample as compared with that in the Ce-Cu-SAPO-18 sample, indicating that a more serious decrease in total isolated Cu^{2+} species of Cu-SAPO-18. As shown in data in Table 2, amount (0.069 mmol/g) of the isolated Cu^{2+} species in the D6R of Ce-Cu-SAPO-18 was higher than that (0.047 mmol/g) of Cu-SAPO-18. According to the literature [10], a more amount of Cu^{2+} in the D6R could enhance stability of a zeolitic sample. In addition, the CuO content in the sample after Ce doping was reduced from 0.116 mmol/g of Cu-SAPO-18 to 0.100 mmol/g of Ce-Cu-SAPO-18, indicating that Cu addition reduced the agglomeration of Cu species. Such a phenomenon was more obvious in hydrothermally aged samples (The CuO contents in Cu-SAPO-18-850 and Ce-Cu-SAPO-18-850 samples are 0.169 mmol/g and 0.126 mmol/g, respectively). Therefore, it can be deduced that addition of Ce contributed to stabilization of the Cu^{2+} species in the D6R cage of Ce-Cu-SAPO-18, i.e., Ce doping promoted amount of the Cu^{2+} species to remain stable during the hydrothermal aging process.

Table 2 Amounts of copper species of the samples after quantitative analysis on their H_2-TPR profiles

Sample	Isolated Cu^{2+} (mmol/g)		Total Cu^{2+} (mmol/g)	CuO (mmol/g)
	8MR	D6R		
Cu-SAPO-18[a]	0.050	0.047	0.097	0.116
Cu-SAPO-18-850	0.012	0.032	0.044	0.169
Ce-Cu-SAPO-18[a]	0.040	0.069	0.109	0.100
Ce-Cu-SAPO-18-650	0.038	0.065	0.103	0.109
Ce-Cu-SAPO-18-750	0.028	0.054	0.082	0.120
Ce-Cu-SAPO-18-850	0.025	0.048	0.073	0.126

[a]Data were obtained by our previous research ref. [18]

3.5 EPR Result

The Cu^{2+} species can produce EPR signals, whereas the other Cu species are silent in the EPR responses. The effect of the HAT on amount of the Cu^{2+} ions was explored by the EPR technique, which can be used as a supplement to H_2-TPR. EPR spectra of the samples before and after the HAT are shown in Figs. 5 and 6. As shown in Fig. 5, two Cu^{2+} species (labelled as α and β) were observed in the fresh Cu-SAPO-18 and Ce-Cu-SAPO-18 samples, which were attributed to the isolated Cu^{2+} species in the D6R ($g_{||}$ = 2.42 mT and $A_{||}$ = 124 G) and those in the CHA cage ($g_{||}$ = 2.36 mT and $A_{||}$ = 122 G) [21], respectively.

As shown in Fig. 6, the hyperfine split associated with the α and β species in Cu-SAPO-18 became significantly weaker after the HAT at 850 °C. Moreover, a new Cu^{2+} ions (labelled as γ) appeared, which was attributed to the Cu^{2+} species on Al_2O_3 ($g_{||}$ = 2.35 mT and $A_{||}$ = 126 G) [22], a result probably due to destruction of the zeolitic crystal structure. For Ce-Cu-SAPO-18, both α and β species had little change and almost no γ species appeared after the HAT at 850 °C. Obviously, more amounts of the α and β species in the Ce-doped samples were retained after the HAT, indicating that amount of the isolated Cu^{2+} species in the D6R of the Ce-Cu-SAPO-18 sample was more than that of the Cu-SAPO-18 sample, which was in good agreement with the H_2-TPR results. After adding Ce to Cu-SAPO-18, the increase in amount of the Cu^{2+} species in the D6R cage of Ce-Cu-SAPO-18 might be a result due to the interaction between Ce and Cu species, which promoted stability of Ce-Cu-SAPO-18 after the HAT process.

3.6 Changes of Acidity

NH_3-TPD experiments were conducted to evaluate acidic sites of the samples before and after the HAT, and their profiles are shown in Fig. 7. There were three desorption peaks. Peak A at lower temperatures (190–220 °C) was assigned to physical adsorption of the NH_3 or adsorption of the

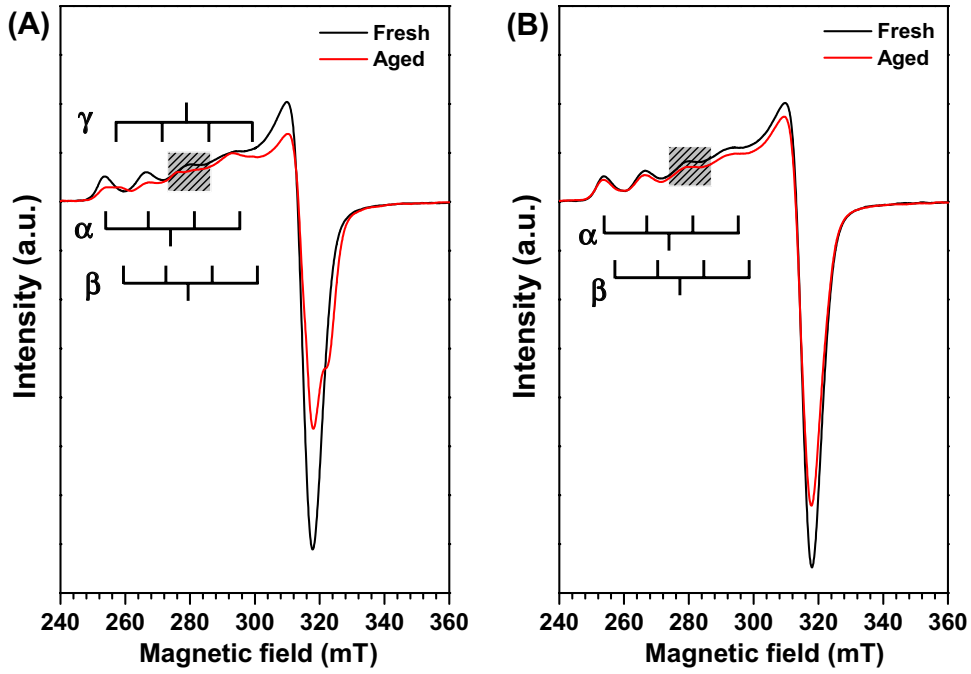

Fig. 5 EPR spectra of **a** Cu-SAPO-18 and **b** Ce-Cu-SAPO-18 before and after the hydrothermal aging treatment at 850 °C

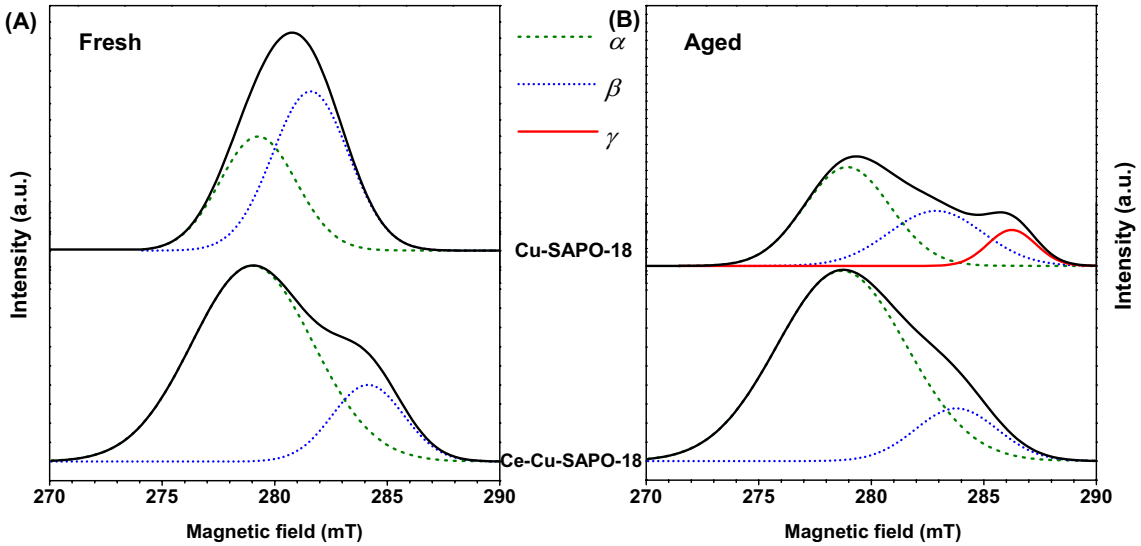

Fig. 6 Deconvolution of EPR spectra of the **a** fresh and **b** 850 °C-aged Cu-SAPO-18 and Ce-Cu-SAPO-18 samples

NH_3 on the surface hydroxyl groups (Si−OH, P−OH, and Al−OH) [23]. Peak B at medium temperatures (250–300 °C) was attributed to the Lewis acid sites produced by the isolated Cu^{2+} species [24]. The peak at higher temperatures (450–500 °C) belonged to adsorption of the NH_3 at the strong Brønsted acid sites [23]. Table 3 lists the acid amounts of the samples.

Figure 7a shows NH_3-TPD profiles of the Ce-Cu-SAPO-18 samples before and after the HAT at different temperatures. After the HAT at different temperatures, amount of each type acidic sites of the Ce-Cu-SAPO-18 sample decreased, and the changes in amount of total acidic sites were in the order of Ce-Cu-SAPO-18 (0.584 mmol/g) > Ce-Cu-SAPO-18-650 (0.556 mmol/g) > Ce-Cu-SAPO-18-750 (0.546 mmol/g) > Ce-Cu-SAPO-18-850 (0.445 mmol/g). Apparently, amount of the acidic sites in the sample decreased when the HAT temperature rose. For example, amount of the acid sites in the fresh Ce-Cu-SAPO-18 sample decreased from 0.546 to 0.445 mmol/g after the sample was hydrothermally aged at 850 °C, which might be due to the structural damage during the high-temperature HAT process. Amount of the total acid sites in the Cu-SAPO-18 sample

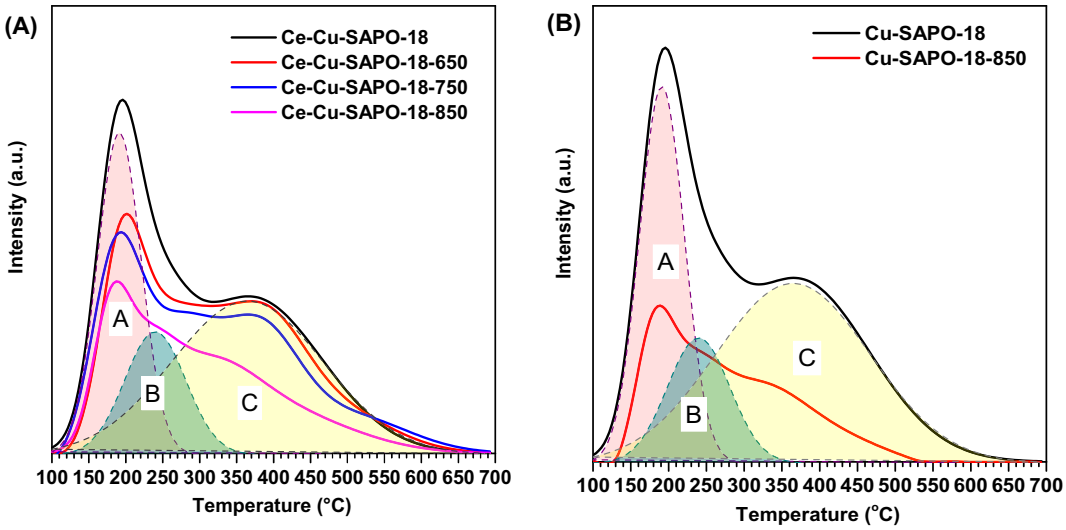

Fig. 7 NH_3-TPD profiles of the fresh and hydrothermally aged Cu-SAPO-18 and Ce-Cu-SAPO-18 samples

Table 3 Acidity of the samples obtained from their NH_3-TPD profiles

Sample	Acidity (mmol/g)			Total acidity (mmol/g)
	Weak	Moderate	Strong	
Cu-SAPO-18[a]	0.204	0.101	0.329	0.634
Cu-SAPO-18-850	0.071	0.076	0.224	0.371
Ce-Cu-SAPO-18[a]	0.107	0.159	0.318	0.584
Ce-Cu-SAPO-18-650	0.112	0.129	0.315	0.556
Ce-Cu-SAPO-18-750	0.124	0.114	0.308	0.546
Ce-Cu-SAPO-18-850	0.143	0.091	0.211	0.445

[a]Data were obtained by our previous research ref. [18]

significantly decreased from 0.634 to 0.371 mmol/g after the HAT at 850 °C. Obviously, amount of the acidic sites in Cu-SAPO-18 decreased much more significantly than that in Ce-Cu-SAPO-18. Additionally, amount (0.091 mmol/g) of the Lewis acid sites formed by the isolated Cu^{2+} species in the Ce-Cu-SAPO-18-850 sample was also more than that (0.076 mmol/g) in the Cu-SAPO-18 sample, indicating that there was still presence of many isolated Cu^{2+} species in Ce-Cu-SAPO-18 after the HAT at 850 °C, which was in good agreement with the H_2-TPR results. In other words, doping Ce could inhibit destruction of the acidic sites in the sample after the HAT, as proven by the above XRD and ^{27}Al MAS NMR results.

3.7 NH_3 Adsorption Ability

NH_3 adsorption properties of the samples before and after the HAT were characterized by the in situ DRIFTS technique. The DRIFTS spectra of all samples are shown in Fig. 8. It can be seen that all of the samples displayed

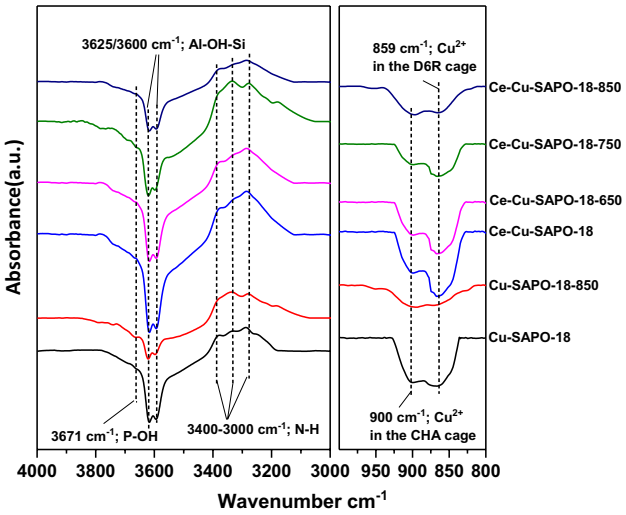

Fig. 8 The DRIFTS spectra of the NH_3-saturated Cu-SAPO-18, Ce-Cu-SAPO-18, Ce-Cu-SAPO-18-650, Ce-Cu-SAPO-18-750, and Ce-Cu-SAPO-18-850 samples. Experimental conditions: the samples were exposed to 500 ppm NH_3 in N_2 at 150 °C for 30 min, and the total flow rate was 100 mL/min

characteristic bands at 3671, 3625, 3600, 3400–3000, 910, and 840 cm^{-1}. The bands at 3671, 3625, and 3600 cm^{-1} were attributed to the NH_3 adsorbed on the P−OH, Al−OH, and Si−OH [12, 20], respectively, which were the characteristic Brønsted acid sites in the 8MRs cage [10, 12]. Additionally, the band at 3000−3400 cm^{-1} was assigned to the N−H bonds [21]. The two negative bands at 840 and 908 cm^{-1} were due to the tetrahedral cation−oxygen−tetrahedral cation (T−O−T) framework vibrations of the samples [12, 20]. The band at 840 cm^{-1} was associated with the Cu^{2+} ions in

the D6R, and the one at 910 cm^{-1} was due to the Cu^{2+} ions in the 8MRs [20, 22]. Intensity of all of the bands assignable to the NH_3 adsorption on the samples after the HAT decreased with different extents, which was consistent with the H_2-TPR and NH_3-TPD results (Fig. 7 and Table 3).

As the hydrothermal temperature rose, intensity of the bands at 3671, 3625, and 3600 cm^{-1} became weaker. In particular, when the temperature rose to 850 °C, intensity of these bands decreased the most obviously, indicating that the Brønsted acid sites in the sample were significantly reduced after the HAT at 850 °C. Intensity of the band at 840 and 908 cm^{-1} also became weaker with the rise in hydrothermal aging temperature, indicating that amount of the isolated Cu^{2+} species in the D6R and 8MR of the samples decreased as the hydrothermal aging temperature increased. Particularly, band intensity of the Cu-SAPO-18 sample was weakened more seriously, as compared with that of the Ce-Cu-SAPO-18 sample after the HAT at 850 °C. It can be found from the above results that NH_3 adsorption capacity of Ce-Cu-SAPO-18 was higher than that of Cu-SAPO-18 after the HAT at 850 °C and introduction of Ce weakened damage of the acidic sites in the samples during the hydrothermal aging process.

4 Discussion

The results of activity evaluation indicate that Ce doping could improve NH_3-SCR performance and hydrothermal stability of the Cu-SAPO-18 catalyst. Compared with Cu-SAPO-18-850, Ce-Cu-SAPO-18-850 retained a higher surface area, a better crystal structure, and less severe dealumination (Figs. 1–3). This result indicates that addition of Ce weakened hydrolysis of the zeolitic sample during the HAT process, thus allowing the zeolitic structure to be mainly retained. Fan et al. [20] reported that Ce addition could effectively reduce the hydrothermal aging dealumination process of the catalyst, while Zhao et al. [24] claimed that the addition of rare earth elements increases the Al content of the zeolitic framework and hence stabilize the Al in the zeolitic frame. From the results of H_2-TPR and EPR characterization (Figs. 4, 5 and Table 2), it can be found that amount of the isolated Cu^{2+} ions in the D6R cage of Ce-Cu-SAPO-18 was more than that of Cu-SAPO-18. According to the literature [10], the isolated Cu^{2+} species in the D6R were more stable than the isolated Cu^{2+} species in the 8MR, which also made the isolated Cu^{2+} in Ce-Cu-SAPO-18 more stable. Therefore, Ce-Cu-SAPO-18 possessed better resistance ability to hydrothermal aging than Cu-SAPO-18. Furthermore, the acid site change in Ce-Cu-SAPO-18 after the HAT was not particularly big and acid sites in the Ce-Cu-SAPO-18 samples were more stable, which might be a result due to that the structure and isolated Cu^{2+} of/in the sample were more stable after Ce doping, allowing acidic sites of the sample to be largely retained after the HAT.

As the HAT temperature rose, deactivation of the Ce-Cu-SAPO-18 sample became serious, which might be caused by the following reasons: As the HAT temperature rose, damage of the zeolitic structure was acumulated to a severe extent, which caused surface area and surface acidity of the sample to decrease, thus leading to drop in activity of the sample (Figs. 2 and 3). With a rise in hydrothermal aging temperature, amount of the isolated Cu^{2+} species in the sample gradually declined (Fig. 4), which might be the main reason for catalyst deactivation. Therefore, it can be concluded that the HAT deactivated the sample by destroying its zeolitic structure, decreasing acidity, and reducing amount of the isolated Cu^{2+} species of/in the sample.

5 Conclusions

Effect of Ce modification on hydrothermal aging property of Cu-SAPO-18 was explored in detail. As compared with Ce-Cu-SAPO-18, Cu-SAPO-18 was more severely destructive after the HAT. After adding Ce, effect of hydrothermal aging on the Cu-SAPO-18 sample became weaker. The reason for the deactivation of Cu-SAPO-18 after the HAT was due to the fact: the Cu^{2+} species in the 8MR cage were easily aggregated to form the aggregated CuO, and further growth of the aggregated CuO destroyed zeolitic structure of the Cu-SAPO-18 sample. Doping of Ce exerted an influence on the zeolitic structure and interaction between the Cu and Ce species. Doping of Ce increased amount of the isolated Cu^{2+} ions in the D6R cage of Cu-SAPO-18, hence making the sample more stable. Ce doping could improve the hydrothermal stability of Cu-SAPO-18 by weakening hydrolysis of the zeolitic structure during the HAT process. Therefore, it is concluded that introduction of Ce could protect the active components (Cu^{2+}) and enhance stability of the zeolitic structure of the Cu-SAPO-18 sample, thereby improving hydrothermal stability of the sample. In addition, as the HAT temperature rose, the zeolitic structure damage of Ce-Cu-SAPO-18 became more serious, resulting in a decrease in catalytic activity.

Acknowledgements This work was supported by the National Natural Science Foundation of China (Grant Nos. 21277008 and 20777005), the National Key Research and Development Program of China (Grant No. 2017YFC0209905), and the Natural Science Foundation of Beijing (Grant No. 8082008). We also thank Prof. Ralph T. Yang (University of Michigan) for his helpful discussion and encouragement.

References

1. Skalska K, Miller JS, Ledakowicz S (2010) Sci Total Environ 408:3976–3989

2. Deka U, Juhin A, Eilertsen EA, Emerich H, Green MA, Korhonen ST, Weckhuysen BM, Beale AM (2012) J Phys Chem C 116:4809–4818
3. Fickel DW, Lobo RF (2010) J Phys Chem C 114:1633–1640
4. Tyrsted C, Borfecchia E, Berlier G, Lomachenko KA, Lamberti C, Bordiga S, Vennestrom PNR, Janssens TVW, Falsig H, Beato P, Puig-Molina A (2016) Catal Sci Technol 6:8314–8324
5. Ma L, Li J, Ke R, Fu L (2011) J Phys Chem C 115:7603–7612
6. Zhang Q, Qiu C, Xu H, Lin T, Lin Z, Gong M, Chen Y (2011) Catal Today 175:171–176
7. Dou B, Lv G, Wang C, Hao Q, Hui K (2015) Chem Eng J 270:549–556
8. Gao F, Washton NM, Wang Y, Kollár M, Szanyi J, Peden CHF (2015) J Catal 331:25–38
9. Shen M, Wen H, Hao T, Yu T, Fan D, Wang J, Li W, Wang J (2015) Catal Sci Technol 5:1741–1749
10. Kim YJ, Lee JK, Min KM, Hong SB, Nam I, Cho BK (2014) J Catal 311:447–457
11. Schmieg SJ, Oh SH, Kim CH, Brown DB, Lee JH, Peden CHF, Kim DH (2012) Catal Today 184:252–261
12. Wang D, Jangjou Y, Liu Y, Sharma MK, Luo J, Li J, Kamasamudram K, Epling WS (2015) Appl Catal B 165:438–445
13. Martínez-Franco R, Moliner M, Corma A (2014) J Catal 319:36–43
14. Ye Q, Wang L, Yang RT (2012) Appl Catal A 427–428:24–34
15. Bin F, Wei X, Li B, Hui KS (2015) Appl Catal B 162:282–288
16. Chen JS, Wright PA, Thomas JM, Natarajan S, Marchese L, Bradley SM, Sankar G, Catlow CR, Gaiboyes PL, Townsend RP, Lok CM (1994) J Phys Chem 98:10216–10224
17. Han S, Cheng J, Zheng C, Ye Q, Cheng S, Kang T, Dai H (2017) Appl Surf Sci 419:382–392
18. Han S, Cheng J, Ye Q, Cheng S, Kang T, Dai H (2019) Micropor Mesopor Mat 276:133–146
19. Zhang T, Qiu F, Li J (2016) Appl Catal B 195:48–58
20. Fan J, Ning P, Wang Y, Song Z, Liu X, Wang H, Wang J, Wang L, Zhang Q (2019) Chem Eng J 369:908–919
21. Xue J, Wang X, Qi G, Wang J, Shen M, Li W (2013) J Catal 297:56–64
22. Wang J, Yu T, Wang X, Qi G, Xue J, Shen M, Li W (2012) Appl Catal B 127:137–147
23. Wang L, Li W, Qi G, Weng D (2012) J Catal 289:21–29
24. Zhao Z, Yu R, Shi C, Gies H, Xiao F, De Vos D, Yokoi T, Bao X, Kolb U, McGuire R, Parvulescu A, Maurer S, Müller U, Zhang W (2019) Catal Sci Technol 9:241–251